Earth and Planetary Science Letters 317-318 (2012) 354–362

Contents lists available at SciVerse ScienceDirect

Earth and Planetary Science Letters

journal homepage: www.elsevier.com/locate/epsl

Glacier longitudinal profiles in regions of active uplift

Rachel M. Headley *, Gerard Roe, Bernard Hallet

Dept. of Earth and Space Sciences, University of Washington, Box 351310, Seattle, WA 98195, United States

ARTICLE INFO

Article history:
Received 9 September 2011
Received in revised form 15 November 2011
Accepted 16 November 2011
Available online 7 January 2012

Editor: T.M. Harrison

Keywords:
glacial erosion
steady-state modeling
surface processes
fjord
glacial geomorphology

ABSTRACT

We combine a simplified equation for ice flow with several proposed glacial erosion laws to solve for longitudinal profiles of glaciers in topographic steady state based on prescribed patterns of rock uplift. The solutions produce realistic looking glaciers and are consistent with previous numerical results. Scaling relationships for the dependence of ice thickness and surface slope on rock uplift and climate (in the form of an imposed ice flux) emerge from the solutions. The general patterns of these dependencies are robust. The ice thickness is dependent upon the ice flux and inversely dependent upon the rock uplift, while the surface slope is inversely dependent upon the ice flux and dependent upon the rock uplift. Different erosion laws lead to only subtle differences in these slope and thickness dependencies. Despite the simplicity of the physics, a first-order match to an actual, over-deepened fjord profile can be obtained. The results provide a theoretical basis for understanding the shape of glacier profiles in tectonically active landscapes, can be used to benchmark numerical models of glacial erosion, and can readily be incorporated directly into simple models of orogen dynamics.

1. Introduction

Glacial erosion is responsible for some of the most spectacular orogens on Earth, including the classic examples of southeastern Alaska, the Patagonian Andes, and New Zealand's Southern Alps. Recent numerical models of landscape evolution have begun to incorporate glacial erosion (Braun et al., 1999; Herman and Braun, 2008; Kessler et al., 2008; Tomkin and Braun, 2002). However, unlike the situation for fluvial erosion, there currently exists no simple analytical framework for examining the steady-state longitudinal profiles of glacier surfaces and valleys. Such a framework would be helpful, for example, to develop insight into the interactions among climate, erosion and uplift, and to understand and evaluate the results of complex numerical models. This study presents such a framework using a few simple, physically-based glacial erosion laws. We address several questions: 1) Can steady-state solutions that combine equations for glacial erosion and flow capture known properties of glacier profiles for some simple case studies? 2) Do different erosion laws produce distinctly different valley forms (longitudinal profiles)? 3) Are large-scale longitudinal profiles of actual glacial valleys and fjords comparable to our theoretical results?

Models of orogenic evolution must average and parameterize erosional processes that act on significantly shorter time- and length-scales, instead of explicitly accounting for them. In the case of glacial erosion there are a several interacting mechanisms with relevant time scales that as short as hours and length scales as small as centimeters, among them: abrasion (Hallet, 1979, 1981; Iverson, 1995), quarrying (Hallet, 1996), and subglacial hydrologic processes (Hooke, 1991; Iverson, 1991; Riihimaki et al., 2005). When glacial erosion is studied at the scale of a whole glacier, or glacier system, the erosion rate is often assumed to simply scale with either the sliding speed (Braun et al., 1999; Herman and Braun, 2008; MacGregor et al., 2000, 2009; Tomkin and Braun, 2002) or flux per unit width (Anderson et al., 2006; Kessler et al., 2008).

Glacial erosion has been implemented in models of mountain-belt development. Tomkin and Roe (2007) studied the pattern of glacial erosion of a critical wedge (where the crust acts as a Coulomb plastic material and maintains a constant slope), but the form of the glacier valley was not a focus, as it is here. MacGregor et al. (2000, 2009) and Anderson et al. (2006) studied the long profiles of glacier valleys using numerical models, in passive landscapes that did not include rock uplift. Our results do include the pattern of rock uplift, and also provide insight applicable to these numerical results. In particular, we develop scaling relationships that show how such results depend on different formulations of the erosion law. A further value of the analytical profiles in the present study is that they do not suffer from any issues regarding numerical resolution or method of solution.

Our derivation of the steady-state form of glacier valley long profiles is closely analogous to classic derivations of steady-state fluvial valley profiles. Fluvial erosion is typically parameterized by some form of river incision law, representing erosion rate as scaling with stream power or basal shear stress (Howard et al., 1994; Seidl and Dietrich, 1993; Sklar and Dietrich, 1998; Whipple and Tucker, 1999). From such assumptions

* Corresponding author at: Institut für Geowissenschaften, Universität Tübingen, Wilhelmstrasse 56, 72074 Tübingen, Germany. Tel.: +49 7071 29 73444; fax: +49 7071 29 5059.
E-mail address: rachel.headley@uni-tuebingen.de (R.M. Headley).

0012-821X/$ – see front matter © 2011 Elsevier B.V. All rights reserved.
doi:10.1016/j.epsl.2011.11.010

arise predictions of how stream slope and area can be related to patterns of precipitation and rock uplift. For instance, the characteristically concave-up shape of river profiles can be understood as being fundamentally driven by the dependence of fluvial incision on the product of discharge and slope. The empirically-derived laws hold even though the exact physical mechanism or physical parameters are only poorly understood or constrained. The intent of this study is to identify whether a similar level of understanding can be applied to glacier profiles. There are some differences: for one, whereas the fluvial case focuses only on the riverbed profile, the glacial solution must predict both the bed and surface topography of the glacier.

To investigate steady-state glacier profiles, we start by developing analytical solutions for ice thickness and surface slope that depend upon climate and tectonic parameters. A variety of erosion laws are presented and discussed. A few simple case studies focusing on a small reach of a glacier are first investigated. Next, the same equations are used to solve for the steady state topography of the whole glacier profile, and for different patterns of climate, as represented simply by ice flux and rock uplift. Finally, while it is not the intent of this study to simulate actual glaciers or glacial topography in detail, we compare the predicted valley profiles and the profile of a typical fjord that reflects prolonged and repeated glaciations over millions of years.

2. Glacier profile equations

We present the equations used to derive the steady-state long profiles of actively eroding glaciers and their valleys, and we highlight the similarities with the derivation of the classic concave-up profile of mountain rivers as we proceed. To begin with, we consider the situation in which the rate of rock uplift, $U(x)$, and the flux of ice per unit width $F(x)$ are prescribed as simple functions of position, x. This is analogous to deriving fluvial long profiles, where the rate of rock uplift and the water discharge are prescribed as functions of position down the river. We note also that the derivation below could also be generalized to include feedbacks between glacial erosion, ice flux, and rock uplift following, for example, Roe et al. (2002) and Whipple and Meade (2006).

We assume that the ice flow is described by the shallow-ice approximation in one-dimension (e.g., Hutter, 1983). This neglects both longitudinal and lateral stresses, the consequences of which will be discussed later. The depth-averaged velocity $\bar{u}$ can be written as

$$\bar{u} = \bar{u}_d + u_s, \tag{1}$$

where the depth-averaged deformation velocity (u_d) and sliding velocity (u_s) are defined by

$$|u_s| = f_s H^{n-1} \left|\frac{dz_s}{dx}\right|^n, \tag{2}$$

$$|\bar{u}_d| = f_d H^{n+1} \left|\frac{dz_s}{dx}\right|^n, \tag{3}$$

(Oerlemans, 1984; Tomkin and Roe, 2007) where f_s and f_d are the sliding and deformation constants, respectively; H is the ice thickness; and z_s is the elevation of the glacier surface. Hereafter we adopt the standard value of $n=3$ from Glen's flow law for ice (Paterson, 1994). Assuming temperate ice, the deformation constant is $f_d = 7.26\times10^{-5}$ ($\mathrm{yr}^{-1}\,\mathrm{m}^{-3}$), and the sliding constant is $f_s = 3.27$ $(\mathrm{m\,yr})^{-1}$ following Tomkin (2003) and Tomkin and Roe (2007). Both f_s and f_d terms depend upon: g, gravitational acceleration ($9.8\,\mathrm{m\,yr}^{-2}$); ρ_i, the density of ice ($910\,\mathrm{kg\,m}^{-3}$); and a sliding A_S or deformation factor A_T, respectively. A_S is taken to match empirical and laboratory data ($1.8\times10^{-16}\,\mathrm{Pa}^{-3}\,\mathrm{yr}^{-1}\,\mathrm{m}^{-2}$) (Bindschadler, 1983; Budd et al., 1979). A_T is an empirical flow factor that is dependent upon temperature relative to the pressure melting point, as well as ice grain size, fabric and impurity content. Following common practice for temperate glaciers, we treat it as a constant ($5\times10^{-16}\,\mathrm{Pa}^{-3}\,\mathrm{yr}^{-1}$) (Paterson, 1994) and this dictates the value for f_d. Given our choices of f_s and f_d, for most of the profiles shown, sliding and deformation are approximately equally important, though we also consider end-member cases where either sliding or deformation is dominant.

The depth-averaged velocity can be related to the flux F by

$$F = \bar{u}H. \tag{4}$$

Combining Eqs. (1)–(4) yields the flux in terms of only the slope, thickness, and flow constants:

$$F = H^3 \left|\frac{dz_s}{dx}\right|^3 \left(f_d H^2 + f_s\right). \tag{5}$$

We now turn to the erosion rate $\dot{e}$. A standard assumption is that the erosion rate scales with the sliding rate raised to the power l:

$$\dot{e} = K(u_s)^l, \tag{6}$$

where $l=1$ is typically assumed, and K represents the bedrock erodibility (e.g. Hallet, 1996; Harbor, 1992; Humphrey and Raymond, 1994). Other values of l can be explored, as is discussed at the end of this section and in Section 3.2.2.

By introducing the topographic steady-state constraint that the erosion rate equals the prescribed rock uplift rate, $\dot{e}=U$, and combining Eqs. (2) and (6), the rock uplift rate can be expressed as a function of only the glacier thickness and ice surface slope:

$$U = K f_s H^2 \left|\frac{dz_s}{dx}\right|^3. \tag{7}$$

By dividing Eq. (5) by Eq. (7), dz_s/dx is eliminated, and the glacier thickness can be expressed only in terms of the rock uplift rate and ice flux:

$$\frac{FK}{U} = \left(\frac{f_d}{f_s}H^2 + 1\right). \tag{8}$$

The limiting proportionalities of Eq. (8) can easily be explored, assuming the constants (K, f_d, and f_s) are spatially uniform. In the case that sliding dominates the ice flow ($f_d H^2 << f_s$), then $H \propto FU^{-1}$. In the case that deformation dominates ($f_d H^2 << f_s$), then $H \propto F^{1/3}U^{-1/3}$. For most of the examples given, the motion of the glacier is a mixture of sliding and deformation, and the ice thickness lies somewhere between these two end members.

Having obtained H, dz_s/dx can be found from Eq. (7) and integrated from x_0 to L to solve for the ice surface elevation z_s using a reference bed elevation $z_0 = z_b(x_0)$:

$$z_s(x) = z_0 + H(x_0) + (Kf_s)^{\frac{1}{3}} \int_{x_0}^{L} \left(\frac{H^2}{U}\right)^{\frac{1}{3}} dx', \tag{9}$$

where x' is a dummy variable of integration and the negative sign accounts for the average negative surface slope as z_s decreases with distance from the head of the glacier towards the toe. Once the ice surface topography has been found, the full profile of bed topography, $z_b(x)$, is simply $z_b(x) = z_s(x) - H(x)$. Note that the thickness and surface slope do not depend upon the choice of z_0.

We consider two other existing formulations for glacial erosion rate. The first is a representation of abrasion (Hallet, 1979; Iverson, 1995; MacGregor et al., 2009)

$$\dot{e} = K_A(u_s)^2, \tag{10}$$

where K_a is an erodibility constant with units of (yr m^{-1}). Secondly we consider the case that glacial erosion scales with the energy dissipated at the bed, or in other words, the basal power

$$\dot{e} = K_P u_s \tau_b, \tag{11}$$

(e.g., Pollard and Deconto, 2007) where K_p represents the erodibility with units of Pa^{-1}, and τ_b is the basal shear stress, which equals $\rho_i g H\, dz_s/dx$.

3. Steady-state profiles

3.1. Illustrative cases

For the first case, we examine the effect of a step decrease in rock uplift rate (Fig. 1a–c). This is an idealization of an active reverse fault underneath a glacier, with differential rock uplift across the fault. We consider a small, central portion of the glacier (L = 5 km), for which ice flux is uniform. The reduction in the rate of rock uplift, and by inferred association the rates of erosion and sliding, drives a reduction in surface slope and a thickening of the glacier (Fig. 1c). The twin constraints represented by Eqs. (5) and (7) must both be satisfied. Physically, Eq. (7) requires that the reduction in rock uplift rate must be balanced by either a reduction in surface slope or thickness (which reduces the sliding and thus the erosion), or some combination of both. However the ice flux is stipulated as constant, and Eq. (5) precludes both dz_s/dx and H reducing at the same time. Thus the reduction in dz_s/dx must be large enough to reduce the sliding velocity despite the effect of the thickening that must accompany it.

The second case examines the effect of a step increase in flux (Fig. 1d–e). An increase in ice flux thickens the glacier and very slightly shallows the slope. The same physical trade-offs described above apply here: the increase in flux could be balanced by either an increase of thickness or an increase in slope, however they are constrained to co-vary in a way that maintains a constant erosion rate. The results are similar to the step in the bed profile and reduction in slope that occurs when the ice flux increases where a tributary glacier merges into another glacier, as modeled numerically by MacGregor et al. (2000).

The magnitude of the changes in H and dz_s/dx are governed by the scaling relationships implied by Eqs. (5) and (7) for the standard erosion rule (6). Table 1 presents the exponents in these scaling relationships for the limits of deformation-dominated and sliding-dominated glacier motion for not only this erosion rule but also for the abrasion (Eq. (10)) and glacier power (Eq. (11)) laws. For the cases shown in Fig. 1, deformation and sliding are equally important, and so the changes in H and dz_s/dx are intermediate between the limits given in the table. In all cases, H scales with a positive exponent on F and negative on U, while the reverse is true for dz_s/dx. It is noteworthy that the scaling exponents in Table 1 are rather insensitive to the choice of erosion law. Among the different laws, the biggest difference is the exponent for U, which is twice as large for the abrasion law as those for the other two erosion laws. This is a direct consequence of the two-fold difference in the sliding velocity exponent in the respective erosion laws.

3.2. Whole glacier profiles

We next present long profiles covering virtually the entire glacier length. The very ends of the glacier must be treated separately. Physically, Eqs. (5) and (7) cannot govern the glacier's behavior through the whole domain. Near the head and toe of the glacier, the thickness must tend to zero. To maintain a non-zero erosion rate, Eq. (7) requires that the slope becomes infinite, which is obviously unphysical, not to mention incompatible with the shallow ice approximation. Thus, this model does not address these end regions for any of the erosion laws (Eqs. (6), (10), and (11)).

This situation is analogous to the fluvial long-profiles. Near the drainage divide, discharge vanishes, and stream-power erosion laws predict that the river slope becomes infinite. In nature, there is a transition down from the divide, from colluvial processes to fluvial processes; for glaciers there is a parallel progression from periglacial processes on steep headwalls and bedrock hillslopes to subglacial

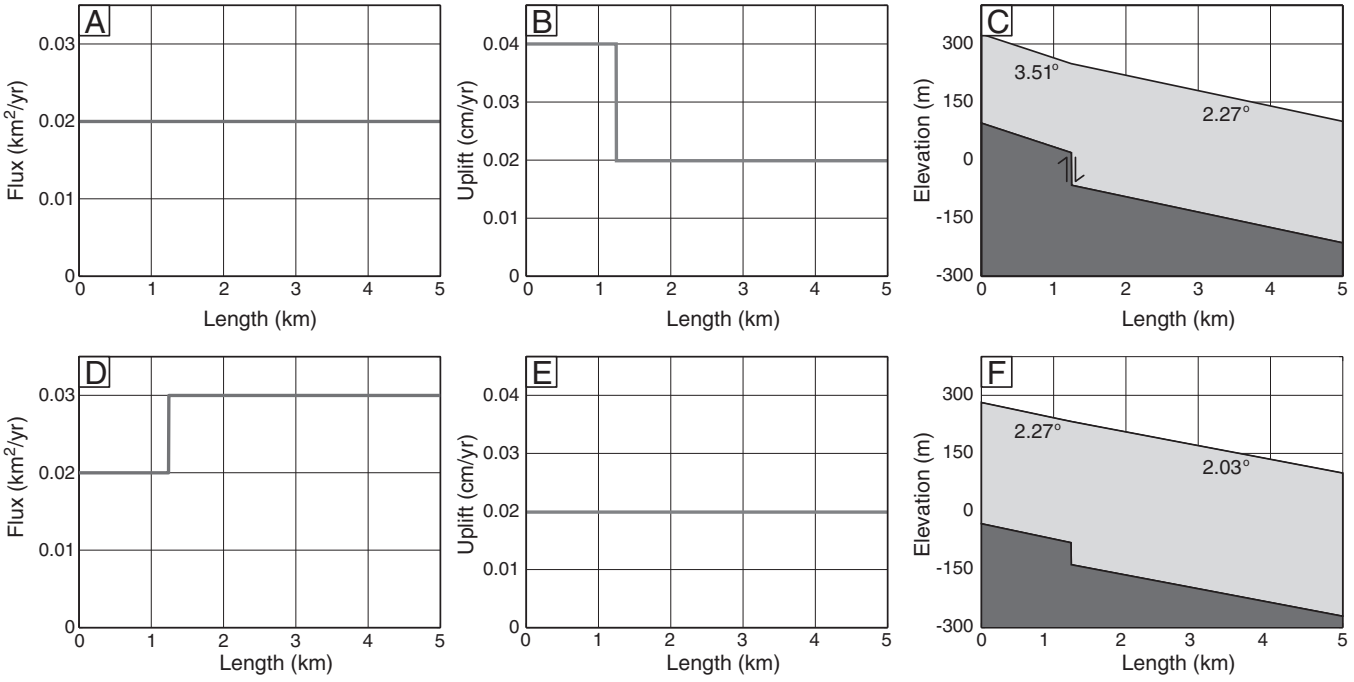

Fig. 1. Simple cases with uniform and step-function properties. The erodibility term, K, is set equal to 10^{-4} so that 20 m yr^{-1} of sliding is equivalent to 2 mm yr^{-1} of erosion, and the reference surface elevation at $x = 5$ km is set at 100 m. A–C show the effects of a step in rock uplift: (A) uniform flux, (B) a step drop in rock uplift and (C) the resulting glacier profile (light gray) and bed (dark gray). The value of the surface slope is also given for each segment of the profile. D–F show the effects of a step increase in flux: (D) step-change in flux, (E) uniform rock uplift, and (F) the resulting glacier (light gray) and bed (dark gray) with the values of the slope labeled for each segment.

Table 1
The thickness and slope scalings for the three different erosion laws for sliding or deformation dominated glacial motion. In general, the contributions of sliding and deformation to the motion of actual glaciers are comparable; hence realistic scalings are expected to be intermediate between these end member models.

	Standard $\dot{e} = K(u_s)$		Abrasion $\dot{e} = K_A(u_s)^2$		Power $\dot{e} = K_P u_s \tau_b$	
Erosion Rule Property	H	$\frac{dz_s}{dx}$	H	$\frac{dz_s}{dx}$	H	$\frac{dz_s}{dx}$
Sliding Dominated: $f_s \ll f_d H^2$	FU^{-1}	$F^{\frac{4}{3}}U$	$FU^{-1/2}$	$F^{-\frac{2}{3}}U^{\frac{1}{2}}$	$F^{-\frac{4}{3}}U^{-1}$	$F^{-1}U$
Deformation Dominated: $f_s \ll f_d H^2$	$F^{\frac{1}{3}}U^{-\frac{1}{3}}$	$F^{-\frac{2}{3}}U^{\frac{5}{3}}$	$F^{\frac{1}{3}}U^{-\frac{1}{6}}$	$F^{-\frac{2}{3}}U^{\frac{5}{6}}$	$F^{\frac{4}{11}}U^{-\frac{3}{11}}$	$F^{-\frac{3}{11}}U^{\frac{5}{11}}$

processes. In models of fluvial erosion, this upper boundary condition is typically represented by a threshold in slope or discharge that is necessary for the onset of fluvial processes (i.e. Howard et al., 1994; Sklar and Dietrich, 1998). At the other end of the fluvial domain there is a downstream transition from fluvial to alluvial or marine processes. In the glacial case, there is a transition from glacial to fluvial processes as the terminus of the glacier is approached.

In the profiles presented here, we choose a simple, slope threshold criterion—we truncate the glacier profiles at locations where the surface slope would exceed 45°. Though the choice of this critical slope is quite arbitrary, it has very little effect on the glacier profiles, and affects less that 2% of the domain. Other choices of boundary condition might be made, but would have little impact on the glacier profiles—the extent of the glacier is essentially determined by the specified glacier mass flux, which reflects the strong constraints set by local climate and the elevation of the glacier in question.

We present multiple glacier profiles. First, we use the standard erosion rule (6). Next, profiles and scaling relationships are presented that compare the other erosion rules (10 and 11). Finally, motivated by empirical studies, two other instructive profiles are presented that make use of the standard erosion rule (6): a more realistic mass balance profile, and a localized zone of high rock uplift

3.2.1. Glacier profile applying the standard erosion rule

As before, we still prescribe the pattern of F and U. The length of the glacier is set as $L = 50$ km. F is specified as a quadratic function equal to 0 at $x = 0$ and $x = L$ (Fig. 2a), representing a flux that results from the integration over the glacier's length of a local mass balance that decreases linearly from $+5\ \mathrm{m\,yr^{-1}}$ at $x = 0$ to $-5\ \mathrm{m\,yr^{-1}}$ at $x = L$. For simplicity a uniform U is specified in this initial case (Fig. 2b). Fig. 2c shows the resulting glacier profile. Starting from the head of the glacier, H increases downslope as the flux of ice increases. To maintain a uniform erosion rate, dz_s/dx must decrease commensurately. Similarly towards the toe of the glacier, H must decrease as the glacier runs out of ice, and dz_s/dx steepens sharply.

As seen in Fig. 2c, the elevation of the glacier ranges from ~1600 m to 3800 m, giving an average slope of less than 5%. The average thickness is approximately 250 m, which is also reasonable for a 50 km glacier. These numbers are quite realistic, building confidence in the premise that a single erosion law based on the physics of glacier flow can apply over all but the very ends of a glacier and that a meaningful erosional steady state can be examined.

3.2.2. Glacier profiles applying other erosion rules

Similar profiles can be calculated for the other erosion laws (i.e., Eqs. (10) and (11)). To compare the different erosion laws, the erodibility constants (K, K_A and K_P) are set such that an erosion rate of $2\ \mathrm{mm\,yr^{-1}}$ occurs for $20\ \mathrm{m\,yr^{-1}}$ of sliding for the sliding-based erosion laws and, for the glacier power rule, the same erosion rate occurs for $20\ \mathrm{m\,yr^{-1}}$ and 10^5 Pa (i.e., 1 bar, being a commonly accepted representative value for basal shear stress of valley glaciers (e.g., Paterson, 1994)). Setting the erodibility constants in this way has precedent from study of fluvial steady states (Whipple and Tucker, 1999). Fig. 3 presents the glacier profiles, with each profile's elevation and length normalized from 0 to 1. In these particular cases, because the rock-uplift rate (U) and the erodibility (K, K_A and K_P) are constants, their values only affect the absolute values of the slope and thickness. In general, when normalized in the way described, the shapes of the profiles (i.e. thickness and slope) depend only on the functional forms of the mass flux and rock uplift, and on the choice of erosion law (Table 1).

Overall the profiles are remarkably similar. In fact, the profiles for the standard and the abrasion erosion laws are identical. The reason is that the scalings of H and dz_s/dx with F are the same, as shown in Table 1. The two laws scale differently with U; so if rock uplift variations were included, the profiles would differ. For the power law, H scales with a larger power of F, and dz_s/dx scales with a more negative power compared to the sliding-based laws. The glacier power law thus produces a generally thicker glacier with a slightly more overdeepened bed.

3.2.3. Glacier profiles motivated by empirical studies

Like the flux of water within a river, the flux of ice within a glacier is influenced by the upstream catchment area. The hypsometry of the glacier matters: for example, the accumulation zone of a glacier is typically much wider than the rest of the glacier, and the mass balance decreases more rapidly with elevation in the ablation area than in the accumulation area. As a result, the ratio of the accumulation area to that of the total glacier (the accumulation area ratio, or AAR) typically ranges from 0.5 to 0.8 (Meier and Post, 1962; Porter, 1977). Anderson et al. (2006), for example, modeled the

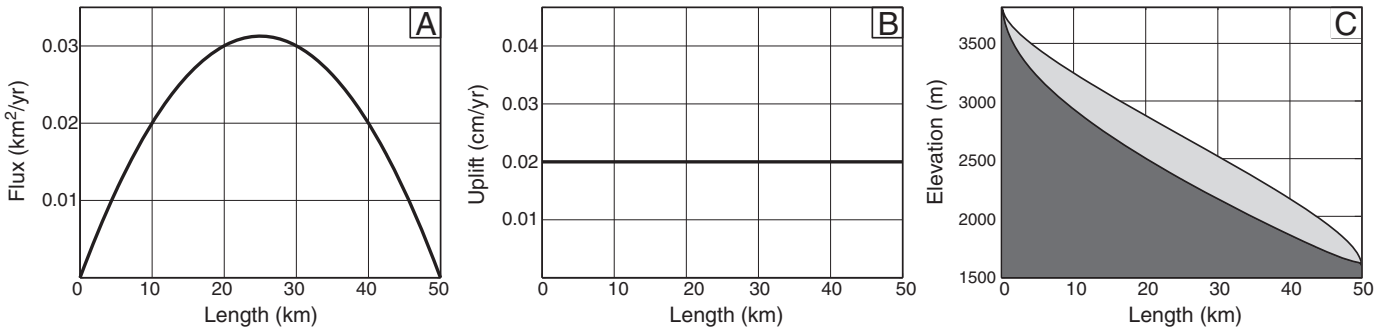

Fig. 2. Simple glacier profile using a parabolic flux (consistent with a linear mass balance profile): A) the flux profile, B) constant rock uplift, and C) the resulting glacier (light gray) and bed (dark gray). See Sections 2 and 3.2 for information about boundary conditions.

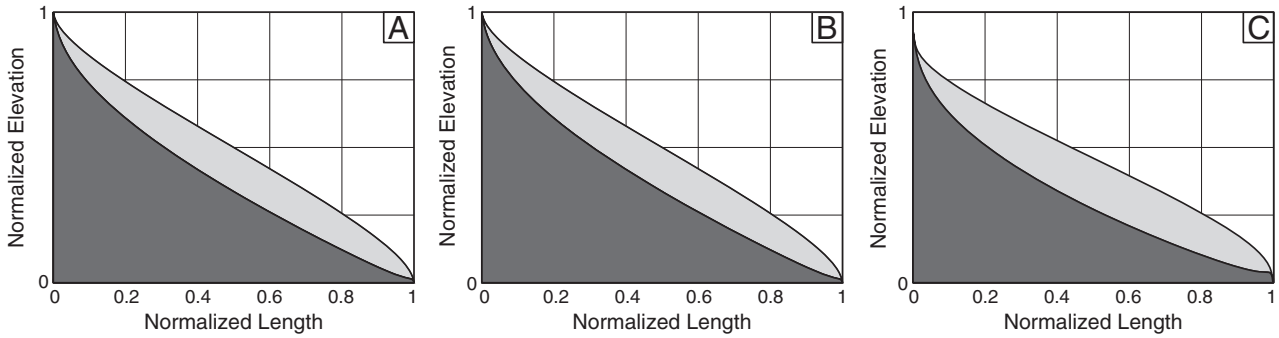

Fig. 3. Normalized glacier (light gray) and bed (dark gray) profiles for different erosion rules using the same parabolic flux and constant rock uplift: A) standard erosion Eq. (6), B) abrasion Eq. (10), and C) power Eq. (11).

profile of a glacier using an ice flux consistent with a high AAR. We consider a similar flux-per-unit-width distribution. The maximum flux is the same as that in Fig. 1a, but its location is skewed toward the terminus of the glacier (Fig. 4a). Fig. 4b shows that, compared to a symmetric flux profile, the resulting glacier profile is thicker toward the toe, as expected given the higher flux there. This results in a bed shape with more excavation towards the toe. Such excavation can cause over-deepenings or basins, which are characteristic of glacier valley profiles (Anderson et al., 2006; Hooke, 1991); they tend to fill with sediments or water to form the wide, flat valley bottoms and lakes that are topographic and landscape signatures of sustained glacial erosion.

The second case study we consider is motivated by recent studies that suggest rapid glacial erosion in the tectonically active St. Elias orogen in SE Alaska (Enkelmann et al., 2009; Spotila et al., 2004). To explore how the subglacial topography and the glacier surface reflect sustained local uplift, we impose a localized zone of rapid rock uplift across the central portion of the glacier. The rock uplift rate is doubled in the center and smoothly decreases to the background over 1 km, representing antiformal uplift (Fig. 5a). The ice flux in this example is uniform. Fig. 5b shows that the higher rock uplift rate creates a transverse ridge in the bed topography, and a thinner and steeper glacier reach above this ridge. The amplitude of the response is governed by the scaling relationships in Table 1—the glacier must thin by a factor between 0.5 (sliding-dominated) and 0.8 (deformation-dominated) relative to the surrounding portions of the glacier; this thinning is manifested in the ridge under the glacier. The surface slope steepens by a factor between 1.5 and 2.0. Fig. 5 also shows the effects, governed by the same laws, of a local decrease in the rock uplift rate, representing crudely an active syncline or graben transverse to the glacier.

3.3. Evaluation over fjord topography

Our steady-state glacier and glacial valley profiles encapsulate the physical principles of orogenic scale glacial erosion, and provide a clear understanding of the consequences of those principles for glacier long profiles. The results also look reasonably similar to actual profiles. However, can these steady-state profiles be compared with real glaciers, and does that constitute a test of the theory? Glaciers are highly transient features on the landscape, fluctuating in response to variations in mass balance (e.g., Roe, 2011; Tomkin, 2009). Due to the intermittent occupation of most glaciated landscapes by ice through the Pleistocene (e.g., Raymo, 1994), valleys have been affected by more than just glacial processes (Ballantyne, 2002; Tomkin, 2009). Nonetheless, there are regions that have been glaciated for geologically significant periods of time. Fjords are glacially carved landforms where the bedrock topography can be constrained readily, and so they offer a possible opportunity for comparisons. Fjords also reflect the combined effects of individual tributaries merging and increasing the ice flux (e.g., MacGregor et al., 2000), the variability in fjord width and sidewall stress, and the variability in the lithology or fracture characteristic of the bedrock that would affect its erodibility. Without attempting to address these small-scale features and without claiming that any specific glacier is in topographic steady state at any given time, we here make a first-order comparison of our predicted profiles with the basal topography of one of the well-known fjords of Norway, Sognefjord.

Sognefjord has a reasonably well-constrained history throughout the Quaternary (Holtedahl, 1967; Nesje and Whillans, 1994). The fjord has been influenced not only by one major trunk glacier but also by many tributary glaciers. While discrete tributary glaciers can in principle be incorporated into the steady-state model, their

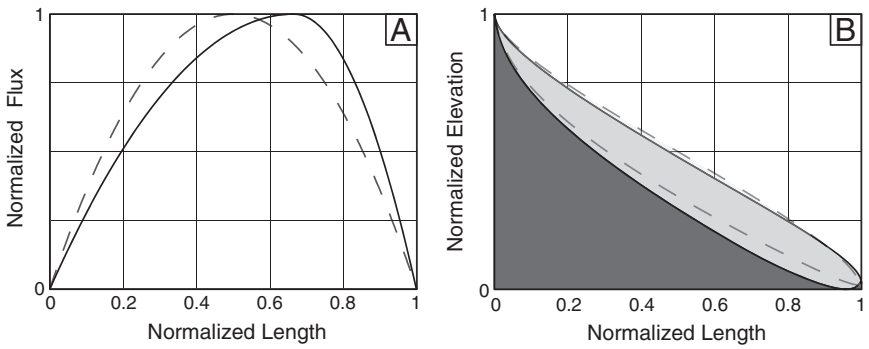

Fig. 4. Simple glacier profile comparing the effect an ice-flux distribution that is parabolic to an ice-flux distribution that is skewed toward the bottom of the glacier. Since valley width is held constant, the skewness is consistent with an accumulation area ratio (AAR) equal to 0.65. Constant rock uplift was used. A) parabolic (dashed) and skewed (solid) flux profiles; B) resulting glacier and bed profiles.

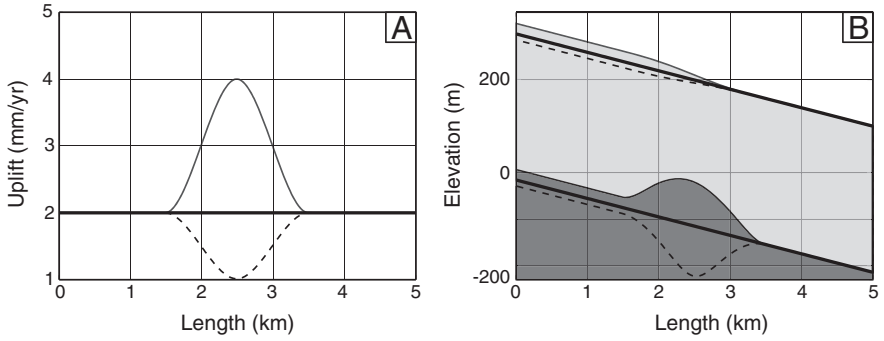

Fig. 5. The effects of local rock uplift and subsidence are shown. The ice flux is spatially uniform at 0.02 km^2 yr^{-1}. A) Imposed spatially uniform rock uplift (thick line), a local doubling (thin solid line) and halving (dashed line) of the rock uplift rate. B) Resulting profiles: local rock uplift (light gray bed, thin solid line), uniform rock uplift (heavy dark lines), and local subsidence (dashed lines).

influence can be represented most simply by a smoothly increasing flux that tapers quickly at the end to represent the calving that likely occurred during the Quaternary glaciations. Only the magnitudes of the ice flux and rock uplift are varied to produce the profile. The flux profile in Fig. 6a starts where the fjord begins and not at the ice divide, hence the flux is non-zero at $x=0$. Moreover, on the high terrain near the ice divide, the glacier was likely frozen to the bed during large glaciations, possibly with insignificant sliding and erosion. In the fjord, the ice was sufficiently thick to assure temperate conditions at the base, hence sliding likely occurred over much of the glacier's history. To make the analysis as simple as possible, we assume that the fjord was continuously occupied and eroded by temperate ice, and we use the sliding erosion rule (6). The flux (Fig. 6a) is found based on a choice of a depth-averaged velocity of 20 m yr^{-1}; this velocity is likely a conservative of glacier velocity averaged over colder and warmer periods. As this has been a relatively tectonically stable region, rock uplift is assumed to be spatially uniform. Using the same erodibility (K) term as in previous examples U is tuned to match an assumed thickness of 1400 m in the deepest portion of the fjord, which is around half of the LGM maximum ice thickness of about 3000 m (Holtedahl, 1967). This gives $U=0.08$ mm yr^{-1}. Fig. 6b shows the resulting glacier profile as well as the actual fjord bathymetry. At the scale of the whole fjord, the profile reproduces

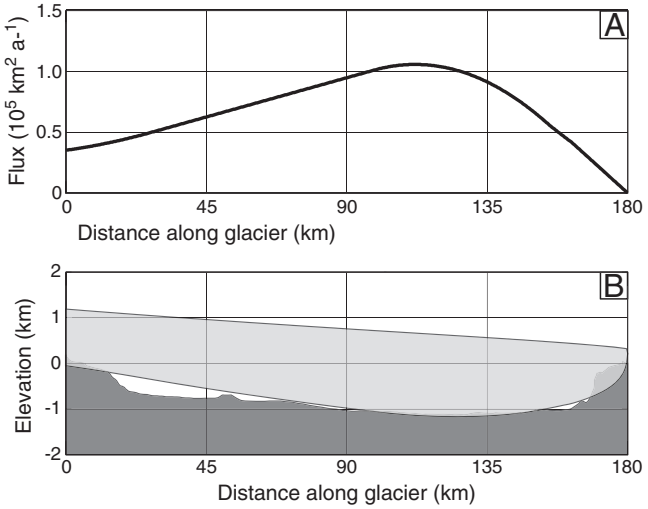

Fig. 6. Comparison of a modeled valley profile to Sognjefjord, Norway. The rock uplift rate is uniform and set at 0.08 mm yr^{-1}. A) Ice flux starts with a non-zero value, representing ice input from highlands into the fjord. The flux peak is skewed toward the end to crudely represent ice loss due to calving. B) The actual fjord profile is compared to the steady state profile produced by the rock uplift and flux.

the average basal slope. It also features a prominent overdeepening at the end of the fjord domain that is similar in scale to the actual fjord, although we note that the actual bedrock base of the fjord (i.e., the depth to which erosion reached) is likely much deeper than the base found from bathymetry due to sediment infilling as the glacier retreated. It is interesting to note that this tendency towards overdeepening occurs without any inclusion of physical processes such as those related to subglacial hydrology or sediment transport, which have been shown to act as limiting agents on smaller glacier profiles (e.g., Alley et al., 2003), though these processes, too, surely act in nature (Herman et al., 2011).

4. Discussion

We present idealized solutions for the steady-state longitudinal profiles of glaciers in tectonically active regions. These solutions are analogous to the classic theory for the steady-state longitudinal profile of rivers, and conceptually it is equivalently simple. When suitable boundary conditions are applied, we find that realistic glacier and valley profiles can be generated for both tectonic and climatic steady state. Reasonable agreement with the theory is also obtained for one well-documented fjord profile. Nonetheless, it is important to recognize that, like the equivalent fluvial theory, the analysis presented here involves considerable idealization of the real world. How might these simplifications affect the analyses? This is discussed in terms of the ice motion and erosional laws, and within the context of transient analyses.

4.1. Ice motion and glacial erosion

We assume that the ice flow is governed by the shallow-ice approximation, which neglects the effects of the longitudinal stresses relative to the shear stresses (Paterson, 1994; Raymond, 1980). While perhaps justified for extensive ice caps, this approximation is generally not valid where longitudinal and lateral stresses are significant. We do, however, show that the basic tendencies of the profiles, as seen in Table 1, are seen in both deformation-dominated and sliding-dominated ice flow. We can therefore be confident that these tendencies will hold provided that the ice flux increases nonlinearly with thickness and down-valley slope, which is still the case even where there are significant longitudinal, lateral (i.e., Pattyn, 2002) and sidewall stresses (i.e., Nye, 1965). For instance, incorporating longitudinal stresses would likely tend to only smooth the change in bed elevation due to vertical displacement across a fault zone (i.e., Fig. 1). A full-stress, flowline model would be an ideal tool for exploring these effects.

The glacier profiles are generated assuming that a single physical process governs erosion along almost the entire glacier. This assumption is common and is made in other numerical models of glacial

erosion (e.g., Anderson et al., 2006; MacGregor, et al., 2000; Tomkin, 2003). We noted that the same rules for both ice flow and erosion could not apply to the very ends of the glacier, as it would lead to an unrealistic profile. Moreover, it is also likely that different erosional processes dominate in various reaches of a glacier. For instance, as meltwater accumulates downglacier due to melting and surface input, subglacial rivers are expected to play an increasing role in eroding the bed (Alley et al., 1997; Dürst Stucki et al., 2010), and in transporting eroded material from beneath the glacier (e.g., Alley et al., 2003). Incorporating simple representations of these processes into our framework is another fruitful area for further work.

We consider several different erosion laws, and find that exponents in the scaling relationships (Table 1) differ by a factor of 2 at most. This is similar to the narrow variation in the exponents governing the dependence of channel slope on discharge and rock uplift for rivers (Gasparini and Brandon, 2011; Whipple, 2004). However, one factor that could be highly variable is the bedrock erodibility, which is in all of the erosion laws, i.e., K in Eq. (6), K_A in Eq. (10), and K_P in Eq. (11). We've assumed the erodibility to be uniform, in common with most models of fluvial erosion (though there are some notable exceptions, e.g., Sklar and Dietrich, 2001). In fluvial field measurements, bedrock erodibility can easily vary by an order of magnitude among different settings (e.g., Whipple and Tucker, 1999). Moreover, it has been suggested that orogen dynamics may be more sensitive to the factors weakening the bedrock (e.g., the tectonic strain and fracture that occur during extreme convergence (Koons et al., 2002; Molnar et al., 2007)) than by the physical processes performing the erosion. For glacial erosion, the erodibility is a function of a variety of physical properties of the bedrock (e.g., fracture spacing, fracture mechanical properties, lithology), and the glacier (basal hydrology, clast content) (e.g., Dühnforth et al., Laitakari et al., 1985; 2010; MacGregor et al., 2009). To the extent that it is meaningful to lump these diverse properties into a single variable that is uniform spatially, the scaling dependence of glacier profile thickness and slope on the erodibility can be calculated using the straightforward method presented in this paper. We note that local variations in erodibility would tend to introduce variability into the relationships we derived, but they would not invalidate our general findings as long as they do not vary in space systematically on the scale of the glacier or orogen length.

Aside from the three erosion rules presented in Eqs. (6), (10), and (11), another commonly invoked law states that the erosion rate is proportional to the ice flux per unit width (Anderson et al., 2006; Kessler et al., 2008). In models that did not incorporate tectonics, Anderson et al. (2006) used this law to investigate glacier valleys, and Kessler et al. (2008) used the law to investigate fjord formation though an existing ridge. For this type of erosion law, a glacial-tectonic steady state cannot be achieved, except in the specific (and unlikely) case that the pattern of ice flux exactly matches the pattern of rock uplift rate. A key feature represented by the present analysis is that the shape of the glacier profile affects the pattern of erosion rate in a way that somewhat differs from the pattern of flux.

4.2. Transient conditions

Finally, we have assumed steady-state conditions throughout these analyses. In this regard, glacier profiles are arguably much more problematic than stream profiles. Glaciers are highly transient elements on a landscape, responding sensitively to the waxing and waning of the Pleistocene ice ages. For example, Roe and O'Neal (2009) have shown that kilometer-scale fluctuations of glacier length can occur due to the interannual variability that occurs even in a constant climate. On what timescales can the glacier profiles presented here be regarded as effectively permanent features of the landscape? The step-change in flux or uplift, considered in Section 3.1 and Fig. 1, generated a step in bed elevation of a few tens of meters, and for the whole glacier (Section 3.2 and Fig. 2), the glacier carves a bed topography that deviates from a uniform slope by about 200 m or so. Dividing these differences in bed profiles by uplift and erosion rates of around 2 mm yr^{-1}, yields characteristic timescales of 10,000 to 100,000 yrs. The lower end of this time scale is well within the known lengths of time that glaciers have persisted, and the longer scale is similar to that of the late Pleistocene glacial cycles. Some evidence exists to show that erosional steady state can exist over this time scale: in an observational study, Herman et al. (2010) argue for the Southern Alps are in steady state by comparing erosion rates from glacial cycles to long-term rates.

Although the simulation of real glaciers is not the primary purpose of this study, a reasonable match to the basal topography of Sognefjord is obtained. To what extent can the theoretical profiles here be compared with actual glaciated landscapes? Physical evidence from moraines and even historical images show that small valley glaciers in the modern climate have clearly not been resident in their current form long enough to be in equilibrium with their bed topography. The hypsometry of valleys that have undergone repeated glaciations have been analyzed (Brocklehurst and Whipple, 2007; Egholm et al., 2009; Mitchell and Montgomery, 2006) and may provide a basis for comparison of the bed topography, though care is needed to account for post-glacial sediment deposition and/or subsequent fluvial modification (Ballantyne, 2002). More extensively glaciated areas may be more conducive to comparison if glacial cover has been sufficiently prolonged, though detailed information about bed conditions is typically lacking in such areas. Thus, a comparison with real-world settings stands as a formidable challenge that extends to any numerical model of glacial erosion. Except in a few cases it has proven elusive to find landscape metrics of fluvial erosion that unambiguously identify changes in climatic or tectonic setting without relying on local calibrations (Brocklehurst, 2010). Arguably the difficulties are greater for glacial erosion.

The framework here can be easily extended to transient calculations in the case of non-tectonic steady state. For this case, the prescribed climate will dictate the glacier flux and the bed will evolve according to $dz_b/dt = U - \dot{e}$, similar to profiles of rivers found by Whipple and Tucker (1999), where dz_b/dt is the time rate of change of z_b the bed elevation, U is the rock uplift, and $\dot{e}$ is the erosion rate. We expect to see equivalent analogs to transient stream profile behavior such as knickpoint propagation, and a damped response to cycles in base-level drop (e.g., Snyder et al., 2003; Whipple, 2004). Further investigations could be performed to better understand the transition between glacial and fluvial at the toe of the glacier, especially when the glacier length is variable in time.

In models of orogenesis, a point of uncertainty is whether it is tectonics or erosion that sets the pattern of rock uplift. Some models of fluvial relief specify rock uplift patterns, as we have done here, and the role of erosion is then to set the total height of the orogen (e.g., Howard et al., 1994; Roe et al., 2002; Whipple et al., 2000). In contrast, Stolar et al. (2007) showed that for the case of a fluvial landscape sitting atop a critical-wedge orogen, high ridge-valley relief in the interior of an orogen required high rates of rock uplift there. In other words the characteristically dendritic and concave-up nature of fluvial networks was a key player in setting the pattern of rock uplift. We are unaware of any equivalent principle for how (or whether) networks of glaciers might play a similar role. However, in a similar manner to Stolar et al. (2007) and Tomkin and Roe (2007), a critical wedge could be evaluated with the glacier model to investigate the potential effects of glacial erosion on the pattern of exhumation. In this case, incorporating the effects of climate variability on glacial extent would be important for comparing glaciological and orogenic time scales. On the larger scale, the rules presented can be incorporated into a growing suite of simple and flexible models of orogenesis (e.g., Roe and Brandon, 2011; Whipple and Meade, 2006) that include fully-coupled feedbacks between climate, erosion, and tectonics.

5. Summary

The simple framework presented here encapsulates much of the current thinking about the controls on glacial erosion at the scale of an active orogen. To achieve topographic steady-state, the glacier profile must satisfy specified tectonic and climatic conditions. Here we've stipulated the tectonics through the spatial pattern of rock uplift rate, U, and the climate simply through a corresponding spatial pattern of the flux of ice, F, within the glacier. Two equations govern the profile behavior: 1) an equation for ice flux governed by the rheology of the ice and the shape of the glacier, and 2) an equation for the erosion rate in terms of ice flow, for which we consider several commonly-invoked representations. Both of these equations can be expressed in terms of the thickness, H, and surface slope. Having to satisfy these twin constraints allows for the end-member dependencies of H and dz_s/dx to be determined as functions only of F and U (Table 1). Just as the simple fluvial theory provides a useful conceptual framework for understanding the basic cause of concave-up river profiles, this framework provides a useful basis for understanding the consequences of glacial erosion laws for a glacier system consistent with its tectonic and climatic setting.

Acknowledgments

We would like to thank E. Waddington, K. Whipple, Frédéric Herman, and an anonymous reviewer, all of whom provided constructive discussion and helpful advice to guide this manuscript. We thank the editor, T. Mark Harrison. We also thank the National Science Foundation for funding that supported this work (Grant nos. 0409884 and EAR-0735402).

References

Alley, R.B., et al., 1997. How glaciers entrain and transport basal sediment: physical constraints. Quat. Sci. Rev. 16, 1017–1038.
Alley, R.B., Lawson, D.E., Larson, G.J., Evenson, E.B., Baker, G.S., 2003. Stabilizing feedbacks in glacier-bed erosion. Nature 424, 758–760.
Anderson, R.S., Molnar, P., Kessler, M.A., 2006. Features of glacial valley profiles simply explained. J. Geophys. Res. 111, F01004.
Ballantyne, C.K., 2002. Paraglacial geomorphology. Quat. Sci. Rev. 21, 1935–2017.
Bindschadler, R., 1983. The importance of pressurized subglacial water in separation and sliding at the glacier bed. J. Glaciol. 29, 3–19.
Braun, J., Zwartz, D., Tomkin, J.H., 1999. A new surface-processes model combining glacial and fluvial erosion. Ann. Glaciol. 28, 282–290.
Brocklehurst, S.H., 2010. Tectonics and geomorphology. Prog. Phys. Geogr. 34, 357–383.
Brocklehurst, S.H., Whipple, K.X., 2007. Response of glacial landscapes to spatial variations in rock uplift rate. J. Geophys. Res. 112, F02035.
Budd, W.F., Keage, P.L., Blundy, N.A., 1979. Empirical studies of ice sliding. J. Glaciol. 23 (89), 157–170.
Dühnforth, M., Anderson, R.S., Ward, D., Stock, G.M., 2010. Bedrock fracture control of glacial erosion processes and rates. Geology 38, 423–426.
Dürst Stucki, M., Reber, R., Schlunegger, F., 2010. Subglacial tunnel valleys in the Alpine foreland: an example from Bern, Switzerland. Swiss J. Geosci. 103, 363–374.
Egholm, D.L., Nielsen, S.B., Pedersen, V.K., Lesemann, J.E., 2009. Glacial effects limiting mountain height. Nature 460, 884–887.
Enkelmann, E., Zeitler, P.K., Pavlis, T.L., Garver, J.I., Ridgway, K.D., 2009. Intense localized rock uplift and erosion in the St Elias orogen of Alaska. Nature Geosci. 2, 360–363.
Gasparini, N.M., Brandon, M.T., 2011. A generalized power law approximation for fluvial incision of bedrock channels. J. Geophys. Res. 116, F02020.
Hallet, B., 1979. A theoretical model of glacial abrasion. J. Glaciol. 23, 39–50.
Hallet, B., 1981. Glacial abrasion and sliding: their dependence on the debris concentration in basal ice. Ann. Glaciol. 2, 23–28.
Hallet, B., 1996. Glacial quarrying: a simple theoretical model. Ann. Glaciol. 22, 1–8.
Harbor, J.M., 1992. Numerical modeling of the development of U-shaped valleys by glacial erosion. Geol. Soc. Am. Bull. 104, 1364–1375.
Herman, F., Braun, J., 2008. Evolution of the glacial landscape of the Southern Alps of New Zealand: insights from a glacial erosion model. J. Geophys. Res. 113, F02009.
Herman, F., Rhodes, E.J., Braun, J., Heiniger, L., 2010. Uniform erosion rates and relief amplitude during glacial cycles in the Southern Alps of New Zealand, as revealed from OSL-thermochronology. Earth Plan. Sci. Lett. 297, 183–189.
Herman, F., Beaud, F., Champagnac, J.D., Lemieux, J.M., Sternai, P., 2011. Glacial hydrology and erosion patterns: a mechanism for carving glacial valleys. Earth Planet. Sci. Lett. 310, 498–508.
Holtedahl, H., 1967. Notes on the formation of fjords and fjord-valleys. Geogr. Ann. Ser. A. 49, 188–203.
Hooke, R.L.E.B., 1991. Positive feedbacks associated with erosion of glacial cirques and overdeepenings. Geol. Soc. Am. Bull. 103, 1104–1108.
Howard, A.D., Dietrich, W.E., Seidl, M.A., 1994. Modeling fluvial erosion on regional to continental scales. J. Geophys. Res. 99, 13971–13986.
Humphrey, N.F., Raymond, C.F., 1994. Hydrology, erosion and sediment production in a surging glacier—variegated glacier, Alaska, 1982–83. J. Glaciol. 40, 539–552.
Hutter, K., 1983. Theoretical Glaciology. Mathematical Approaches to Geophysics. D.Reidel Publishing Company, Boston.
Iverson, N.R., 1991. Potential effects of subglacial water-pressure fluctuations on quarrying. J. Glaciol. 37, 27–36.
Iverson, N.R., 1995. Processes of erosion. In: Menzies, J. (Ed.), Glacial Environments—Processes, Sediments, and Landforms. Butterworth-Heinemann, Oxford, pp. 241–259.
Kessler, M.A., Anderson, R.S., Briner, J.P., 2008. Fjord insertion into continental margins driven by topographic steering of ice. Nat. Geosci. 1, 365–369.
Koons, P.O., Zeitler, P.K., Chamberlain, C.P., Craw, D., Meltzer, A.D., 2002. Mechanical links between erosion and metamorphism in Nanga Parbat, Pakistan Himalaya. Am. J. Sci. 302, 749–773.
Laitakari, I., Aro, K., Fogelberg, P., 1985. The effect of jointing on glacial erosion of bedrock hills in southern Finland. Fennia 163, 369–371.
MacGregor, K.R., Anderson, R.S., Anderson, S.P., Waddington, E.D., 2000. Numerical simulations of glacial-valley longitudinal profile evolution. Geology 28, 1031–1034.
MacGregor, K.R., Anderson, R.S., Waddington, E.D., 2009. Numerical modeling of glacial erosion and headwall processes in alpine valleys. Geomorphology 103, 189–204.
Meier, M.F., Post, A.S., 1962. Recent variations in mass net budgets of glaciers in western North America. IAHS Publ. 58, 63–77.
Mitchell, S.G., Montgomery, D.R., 2006. Influence of a glacial buzzsaw on the height and morphology of the Cascade Range in central Washington State, USA. Quat. Res. 65, 96–107.
Molnar, P., Anderson, R.S., Anderson, S.P., 2007. Tectonics, fracturing of rock, and erosion. J. Geophys. Res. 112, F03014.
Nesje, A., Whillans, I.M., 1994. Erosion of Sognefjord, Norway. Geomorphology 9, 33–45.
Nye, J.F., 1965. The flow of a glacier in a channel of rectangular, elliptic or parabolic cross-section. J. Glaciol. 5, 661–690.
Oerlemans, J., 1984. Numerical experiments on glacial erosion. Z. Gletscherkd. Glazialgeol. 20, 107–126.
Paterson, W.S.B., 1994. *Physics of Glaciers* Third. Butterworth-Heinemann, Birlington, MA.
Pattyn, F., 2002. Transient glacier response with a higher-order numerical ice-flow model. J. Glaciol. 48, 467–477.
Pollard, D., Deconto, R.M., 2007. A Coupled Ice-Sheet/Ice-Shelf/Sediment Model Applied to a Marine-Margin Flowline: Forced and Unforced Variations. In: Hambrey, M.J., Christoffersen, P., Glasser, N.F., Hubbard, B. (Eds.), Glacial Sedimentary Processes and Products. Blackwell Publishing, Oxford, UK, pp. 37–52.
Porter, S.C., 1977. Present and past glaciation thresholds in the Cascade Range, Washington, USA: topographic and climatic controls, and paleoclimatic implications. J. Glaciol. 18, 101–116.
Raymo, M.E., 1994. The initiation of Northern Hemisphere glaciation. Annu. Rev. Earth Planet. Sci. 22, 353–383.
Raymond, C.F., 1980. Temperate valley glacier. In: Colbeck, C.S. (Ed.), The Dynamics of Snow and Ice Masses. Academic Press, New York, USA, pp. 79–193.
Riihimaki, C.A., MacGregor, K.R., Anderson, R.S., Anderson, S.P., Loso, M.G., 2005. Sediment evacuation and glacial erosion rates at a small alpine glacier. J. Geophys. Res. 110, F03003.
Roe, G.J., 2011. What do glaciers tell us about climate variability and climate change? J. Glac. 57, 567–578.
Roe, G.H., O'Neal, M.A., 2009. The response of glaciers to intrinsic climate variability: observations and models of late-Holocene variations in the Pacific Northwest. J. Glaciol. 55, 839–854.
Roe, G.H., Brandon, M.T., 2011. Critical form and feedbacks in mountain belt dynamics: the role of rheology as a tectonic governor. J. Geophys. Res. 116, B02101.
Roe, G.H., Montgomery, D.R., Hallet, B., 2002. Effects of orographic precipitation variations on the concavity of steady-state river profiles. Geology 30, 143–146.
Seidl, M.A., Dietrich, W.E., 1993. The problem of channel erosion into bedrock. Catena Suppl. 23, 101–124.
Sklar, L., Dietrich, W.E., 1998. River longitudinal profiles and bedrock incision models: stream power and the influence of sediment supply. In: Tinkler, K.J., Wohl, E.E. (Eds.), Rivers Over Rock: Fluvial Processes in Bedrock Channels. : Geophys. Monogr. Ser. AGU, Washington, D. C, pp. 237–260.
Sklar, L.S., Dietrich, W.E., 2001. Sediment and rock strength controls on river incision into bedrock. Geology 29, 1087.
Snyder, N.P., Whipple, Kelin X., Tucker, G.E., Merritts, D.J., 2003. Channel response to tectonic forcing: field analysis of stream morphology and hydrology in the Mendocino triple junction region, northern California. Geomorphology 53, 97–127.
Spotila, J.A., Buscher, J.T., Meigs, A.J., Reiners, P.W., 2004. Long-term glacial erosion of active mountain belts: example of the Chugach-St. Elias Range, Alaska. Geology 32, 501–504.
Stolar, D., Roe, G., Willett, S., 2007. Controls on the patterns of topography and erosion rate in a critical orogen. J. Geophys. Res. 112, F04002.
Tomkin, J.H., 2003. Erosional feedbacks and the oscillation of ice masses. J. Geophys. Res. 108, 2488.
Tomkin, J.H., 2009. Numerically simulating alpine landscapes: the geomorphologic consequences of incorporating glacial erosion in surface process models. Geomorphology 103, 180–188.
Tomkin, J.H., Braun, J., 2002. The influence of alpine glaciation on the relief of tectonically active mountain belts. Am. J. Sci. 302, 169–190.

Tomkin, J.H., Roe, G.H., 2007. Climate and tectonic controls on glaciated critical-taper orogens. Earth Planet. Sci. Lett. 262, 385–397.
Whipple, Kelin X., 2004. Bedrock rivers and the geomorphology of active orogens. Annu. Rev. Earth Planet. Sci. 32, 151–185.
Whipple, K.X., Meade, B.J., 2006. Orogen response to changes in climatic and tectonic forcing. Earth Planet. Sci. Lett. 243, 218–228.
Whipple, Kelin X., Tucker, G.E., 1999. Dynamics of the stream-power river incision model: implications for height limits of mountain ranges, landscape response timescales, and research needs. J. Geophys. Res. 104, 17,661–17,674.
Whipple, K.X., Hancock, G.S., Anderson, R.S., 2000. River incision into bedrock: mechanics and relative efficacy of plucking, abrasion, and cavitation. Geol. Soc. Am. Bull. 112, 490–503.